GA–A26800

THE MULTIPLE GYROTRON SYSTEM ON THE DIII-D TOKAMAK

by
J. LOHR, M. CENGHER, J.L. DOANE, Y.A. GORELOV, C.P. MOELLER, D. PONCE,
and R. PRATER

July 2010

GENERAL ATOMICS

DISCLAIMER

GA–A26800

THE MULTIPLE GYROTRON SYSTEM ON THE DIII-D TOKAMAK

by
J. LOHR, M. CENGHER, J.L. DOANE, Y.A. GORELOV, C.P. MOELLER, D. PONCE, and R. PRATER

This is a preprint of a synopsis of a paper submitted for publication in a Special Issue of *J. Infrared Millimeter Waves and Terahertz*.

Work supported by
the U.S. Department of Energy
under DE-FC02-04ER54698

GENERAL ATOMICS ATOMICS PROJECT 30200
JULY 2010

ABSTRACT

The electron cyclotron heating and current drive complex on the DIII-D tokamak presently comprises six gyrotrons injecting rf power from the low field side at 110 GHz, the $2f_{ce}$ resonance at the center of the vacuum chamber. Typical injected rf power is 600–650 kW per gyrotron. The launched rf can be directed over ±20° toroidally to create both co- and counter-current drive and scanned over 40° poloidally to permit the injected rf beams to intersect, and be absorbed at, the second harmonic resonance anywhere in the tokamak upper half plane. The elliptical polarization is controlled so that the desired extraordinary or ordinary modes are excited for any injection geometry. The maximum injected energy on a single plasma shot has been 16.6 MJ for six gyrotrons injecting a total of 3.4 MW for 5 seconds.

I. INTRODUCTION

There has been a long history of research using gyrotrons as rf sources for electron cyclotron heating and current drive on the DIII-D tokamak and its predecessor the DIII-D tokamak. In the mid-1980s, a 60 GHz 10 gyrotron system rated at 2.5 MW that generated power for up to 1 s pulses was operated. This system was used both for low field side injection and for injection from the high field side to avoid the reflecting right hand cutoff layer. The experiments studied heating effectiveness [1] and current drive [2] and verified many aspects of the theory of wave-particle interactions at the electron cyclotron frequency and its harmonics [3,4]. They were the first to demonstrate an electron cyclotron heating (ECH) driven H-mode discharge [5] and also, unfortunately, demonstrated that encountering the second harmonic resonance in the waveguides, where they crossed the top of the tokamak vacuum vessel to reach the high field side, posed risk of waveguide arcing and damage to the guides. With larger diameter waveguide and better vacuum conditions due to increased pumping speed in the waveguides, arcing in the waveguides at resonant field locations was not observed. High field launch experiments are described in [1]. The H-mode regime was accessed both with fundamental and second harmonic ECH injection at an injected power level of 1 MW [6].

By 1996, the 60 GHz system, limited to operation at relatively low density, had been phased out and a 110 GHz system featuring gyrotrons in the 1 MW class began to be installed [7]. Eventually the installation grew to the present six-gyrotron complex. The histories of the 110 GHz gyrotrons at DIII-D are summarized in Table 1.

In a gyrotron, the high vacuum inside the tube is separated from the outside world by a resonant window through which the microwave beam passes. Initially, no available gyrotron output window material was completely satisfactory for MW class gyrotrons at pulse lengths required for tokamak experiments on DIII-D. The three Gycom* gyrotrons [8] originally used in the DIII-D system had boron nitride (BN) windows and the first high-performance CPI† gyrotron [9] had a double disk sapphire window with face cooling using a chlorofluorocarbon liquid (FC-75) that posed a contamination hazard for the tokamak. For both of these gyrotron types, the rf beam was intentionally broadened [10], reducing the peak power density in order to keep the BN window temperature below its 1000ºC failure point and to avoid thermal runaway of the sapphire windows. The CPI tube generated 1.09 MW for 600 ms pulses at the window limit and the Gycom tubes

*Gycom, Nizhny Novgorod, Russian Federation.

†Communications and Power Industries, Palo Alto, California, USA.

generated about 800 kW for 2 s pulse lengths [11]. Despite the use of phase correcting mirrors [12], it proved to be impossible to recover all the power in the higher order modes required for broadening the beams and the power in the low-loss $HE_{1,1}$ mode in the waveguide was reduced by about 15% as a result. One CPI gyrotron, which began operation in 1998, was a triode gun design producing a Gaussian rf beam. This was the first gyrotron at DIII-D equipped with a chemical vapor deposition (CVD) diamond output window [13]. Despite pH control, the aluminum diffusion bond used to attach the window to its flange corroded when in contact with the cooling water resulting in gyrotron vacuum failure.

Table 1. Summary of the histories of the 110 GHz gyrotrons in the 1 MW class, which have been in service at DIII-D. Only the 1 MW CPI gyrotrons with 5 s pulse capability are presently active in the system at DIII-D. P_{GEN} is the power typically generated during operations and τ is the maximum operational pulse length.

Gyrotron	Manufacturer	Date	P_{GEN}/τ (MW/s)	Operational Status/History
CURRENT DIII-D SYSTEM GYROTRON PARAMETERS				
Scarecrow	CPI	2000	0.85/5	Normal operation. The gyrotron had its window replaced after corrosion failure of the aluminum seal and later had its collector replaced after a large water leak developed.
Tinman	CPI	2000	0.85/5	This gyrotron had a small leak in the bottom of the collector, which limited performance. The tube has been repaired at CPI, conditioned at DIII-D and is in regular service.
Lion	CPI	2002	0.85/5	This gyrotron had a collector failure with substantial overheating, slight buckling of the structure and extensive stress cracking on the hot sides of the cooling tubes. Repair was completed and the gyrotron is in regular service at DIII-D.
Luke	CPI	2005	0.85/5	This gyrotron is in regular, reliable service at DIII-D.
Han	CPI	2006	0.75/5	In regular, reliable service at DIII-D. Power lower than others.
Leia	CPI	2007	0.85/5	This gyrotron is in regular, reliable service at DIII-D
DIII-D RETIRED GYROTRON OPERATIONAL HISTORIES				
Katya	Gycom	1996	0.6/2.0	On standby, not operating; cathode efficiency was slowly decreasing, but operation was reliable with P_{GEN}~600 kW. Katya is semi-retired but could be returned to service if required. May go to KSTAR.
Boris	Gycom	2000	0.75/2.0	Gyrotron removed from service in good condition and installed and operating on KSTAR for break-down assist and transition to equilibrium. P_{GEN}~750 kW with full HV and current.
Natasha	Gycom	2000	0.5/2.0	Retired/vacuum failure. Probably can be repaired if desired.
Chewbacca	CPI	2006	1.3/short	This gyrotron was the first 110 GHz CPI gyrotron with a depressed collector. Chewy completed testing at CPI. 1.25 MW short pulse, >500 kW, 10 s pulses. The tube was installed at DIII-D and being operated at low power without rf generation when it developed a collector leak. The design, with a new CrZrCu collector and other improvements, is the basis for the next gyrotron for DIII-D.

Three new CPI gyrotrons at 110 GHz with designed pulse length of 10 s, producing Gaussian output beams and having a newly developed Au/Cu braze on CVD diamond windows, began to be added to the system in 2000. These tubes generated about 550 kW

for 10 s pulses in half power acceptance tests at CPI and then were tested to 1.0 MW output for 5 s pulse length in final acceptance tests at DIII-D. This group of gyrotrons has diode guns and operates at 80 kV and 40 A. After a period of operation, all three of these gyrotrons developed water leaks into the collectors [14]. The problem was traced to overheating of the collectors during testing and operation with collector power loading of up to 1 kW/cm^2 and subsequent fatigue failure. Re-examination of the thermal fatigue calculations for these OFHC copper collectors showed that this loading was excessive and that maximum loading of 600 W/cm^2 would be required to provide a collector fatigue lifetime of 50,000 5 s pulses at full parameters. To reduce the peak electron beam loading to this lower value, the range of the electron beam sweeping in the collector was increased and the center of the sweep was raised to increase the footprint; the maximum sweep coil voltage was increased to 200 V with a sawtooth waveform to reduce the dwell time at the ends of the sweep; the sweep frequency was increased from 4 to 5 Hz and care was taken to stop the pulse whenever rf generation ceased for a variety of reasons.

The collector fatigue lifetime for short pulses ~200 ms in duration is determined by the total number of pulses and for longer pulses by the actual pulse length because of cyclic heating during sweeping. Collector heating on the CPI gyrotrons in the DIII-D system, measured during operation using an array of 160 evenly distributed RTDs on the outer surface of the collector, Fig. 1, verified that the above measures reduced the time-averaged collector power loading at all points around the collector to ≤ 600 W/cm^2 required by the fatigue calculations. Collector loading measurements with no sweeping, a tilted electron beam and about half maximum generated power in Fig. 1 are compared with a horizontally aligned beam with improved sweeping at full power in Fig. 2. The sequence of changes in the sweep coil waveform from symmetric to sawtooth, which is shown in Fig. 2, is compared with direct magnetic field measurements inside the tube to demonstrate the reduced dwell time at the turnaround point for the sawtooth sweep. The failed collectors were repaired and these tubes were all returned to regular service. A second group of three CPI diode gyrotrons was then installed and the short pulse Gycom tubes with BN windows were retired. One of these Gycom gyrotrons has since been installed on the KSTAR tokamak [15] to help provide breakdown at low loop voltages available in this superconducting tokamak.

The two main difficulties with the initial production tubes were the excessive collector loading and the corrosion in the aluminum diffusion bond on the earliest CVD diamond window, both of which have been addressed successfully. Problems such as multi-kW low frequency parasitic emission [11], cavity overheating, poor rf beam quality and beam tunnel oscillations [16], which have been seen on other MW class gyrotrons, have not been a problem on the CPI tubes at DIII-D. The six gyrotrons in the DIII-D system are now used daily in support of the scientific program.

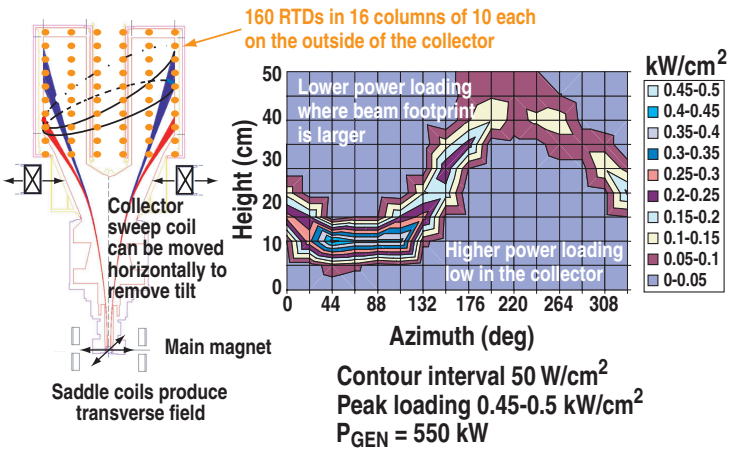

Fig. 1. Measurement of the collector power loading using an array of RTDs on the outer surface of the collector and a model for heat transfer through the OFHC copper. This low power beam is tilted and the measurement demonstrates the size of the electron beam and higher loading low in the collector where the footprint is smaller for a case with no sweeping

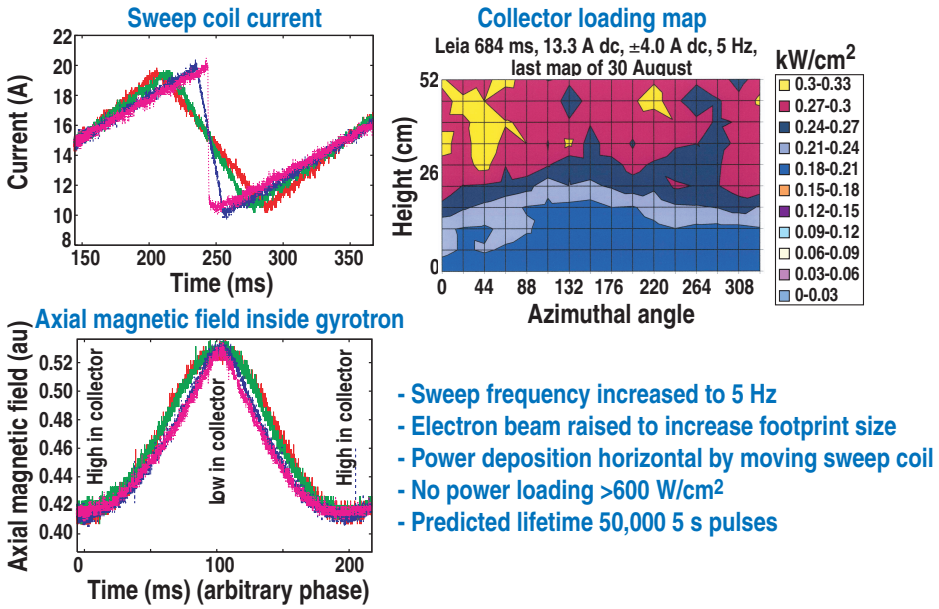

Fig. 2. The copper collector and iron magnetic shield increase the penetration time for the sweep field limiting the maximum sweep frequency, but the sawtooth waveform alone decreases the dwell time low in the collector by about 25% at 5 Hz.

II. HARDWARE OVERVIEW

A. Gyrotron Vault

The gyrotrons [17] on the DIII-D tokamak [18] are installed in a specialized room located about 60 m from the tokamak and each tube is connected to DIII-D by about 90 m of evacuated circular corrugated waveguide, with about 12 miter bends, including the two polarizers, in each line and no isolation windows at the tokamak. The waveguide diameter is 31.75 mm and, because of the relatively high flow impedance provided by this size waveguide, the tokamak is protected against catastrophic vacuum leaks by a combination of the impedance and by gate valves at the tokamak that close in about one second following a vacuum failure. On one occasion a water leak developed in a waveguide dummy load during a gyrotron pulse and the resulting steam loaded the waveguide with water. The protective gate valve closed, the rf pulse was terminated and, despite the need for a subsequent waveguide cleanup, the tokamak pulse terminated normally. When gyrotron windows face-cooled with FC-75 were used, a fast acting shutter was incorporated into the system to protect the tokamak against serious contamination from the chloroflurocarbon in case of a window failure. These shutters closed in less than 100 ms, but, with the advent of CVD diamond windows, were never called upon to perform the protective function and have been removed from the system. For ECH systems using larger diameter waveguides, the passive protection provided to the tokamak by the limited conduction of smaller diameter lines may not be as effective and waveguide windows may be required.

There are competing factors in the design of the installation determining the distance between the gyrotrons and the tokamak. Although longer transmission lines lead to increased losses independent of the number of miter bends, stray magnetic fields from operation of an air solenoid tokamak are reduced with distance. Therefore the magnetic environment can more easily be controlled to reduce the horizontal field components to acceptable levels as the distance from the tokamak is increased. To improve the magnetic geometry at the gyrotrons, which require <0.15% radial magnetic field error out of ~4 T, the floor in the DIII-D gyrotron vault is designed as a magnetic equipotential surface, with no isolated magnetic beams or struts. Placement of the gyrotron cavities at the height of the tokamak midplane also significantly reduces the radial field [19].

B. Waveguide

The waveguides in the DIII-D transmission lines are all made from aluminum, step-corrugated on the inside with corrugation depth $\sim\lambda/4$ and very low fields at the wall, resulting in low loss transmission [20]. The lines vary in length, but average about 90 m

and have an inside diameter of 31.75 mm. This diameter represents a compromise for 3 mm wavelength. Use of larger diameter waveguides, typically 63.5 mm diam., requires careful attention to alignment and support during installation, but has smaller transmission loss, an important consideration for cw operation. The smaller diameter guide used on DIII-D has somewhat higher losses, but functions more like waveguide and can be bent moderately with no change in transmission. Cost is a factor in comparing different diameter waveguide lines, particularly for components such as miter bends, switches and polarizers, which are cheaper for the smaller sized waveguides. At the input end, the rf power is directed from a matching optics unit (MOU) into the waveguides, where smaller waveguide is more sensitive to transverse misalignment and the larger waveguide is more sensitive to tilt misalignment. The intrinsic loss in 90 m of 31.75 mm diameter waveguide at $\lambda = 3$ mm is 2% (-0.09 dB) and is about a quarter of this for the larger 63.5 mm diam. waveguide also commonly used.

The MOU is evacuated by a 250–300 l/s turbomolecular pump, which also pumps both the waveguide to the tokamak and the dummy loads near the gyrotron. A second equivalent turbomolecular pump located near the tokamak evacuates the waveguides from the other end. With this pumping arrangement, the lines can immediately be opened to the tokamak after a waveguide vent and only a few short rf conditioning pulses are required prior to rf injection at full parameters. The waveguide base pressure at the tokamak is about 1.3×10^{-5} Pa under normal circumstances and there has been no evidence of arcing in the lines except near the injection point at the output of the MOU when the alignment was poor.

The rf power can either be routed to DIII-D or, by activating a waveguide switch, into dummy loads. The water-cooled dummy loads comprise a waveguide load, which absorbs about 75% of the power and a backstop load which absorbs the rest. For gyrotrons generating in excess of 1 MW, two waveguide loads are used in series, the first designed to absorb 50% of the power and the second 100% of the remainder. Typically the backstop loads in the DIII-D system absorb about 20% of the injected power since some rf power leaks through the waveguide loads, possibly due its to being in the wrong mode at the input to the dummy loads. The waveguide loads [21], Fig. 3, have a smooth wall section at the input end followed by a short section with taper in the corrugation depth, which converts the propagating $HE_{1,1}$ waveguide mode to the highly damped $EH_{1,1}$ surface wave. The lengths of the smooth wall section and corrugation taper allow the damping fraction to be regulated in a two-step process. The thermal expansion of these loads, about 5 mm, is accommodated by a specialized waveguide bellows section. The loads are extremely black, having the same absorption, >95%, as the plasma itself.

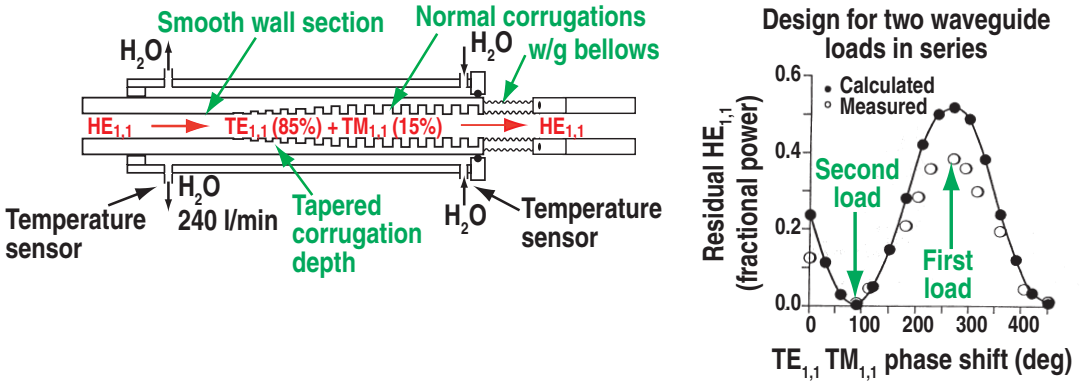

Fig. 3. The waveguide dummy loads convert a fraction of the propagating $HE_{1,1}$ power to higher order modes, which damp in the water-cooled cores. The length of the smooth wall section determines the fraction of converted power. For generated power >1 MW, two of these loads, the first absorbing 50% and the second 100% of the rf power, are used in series. A small backstop load absorbs the remainder of the power. The phase shift between $TE_{1,1}$ and $TM_{1,1}$ modes generated by the smooth wallsation determines the fraction of the rf beam which passes through the load as $HE_{1,1}$ and the absorbed $EH_{1,1}$ mode fraction.

At the tokamak, the six waveguide lines are organized into three groups of two and each group is routed to an articulating launcher, mounted on the tokamak vacuum vessel above the equatorial plane and angled downward so the rf can be injected to cross the second harmonic resonance at its intersection with any flux surface for most tokamak equilibria. The measured profiles of temperature and density are coupled with the equilibrium code EFIT [22] and the injection geometry to provide input to the ray tracing code TORAY [23], which calculates the heating and current drive profiles, Fig. 4.

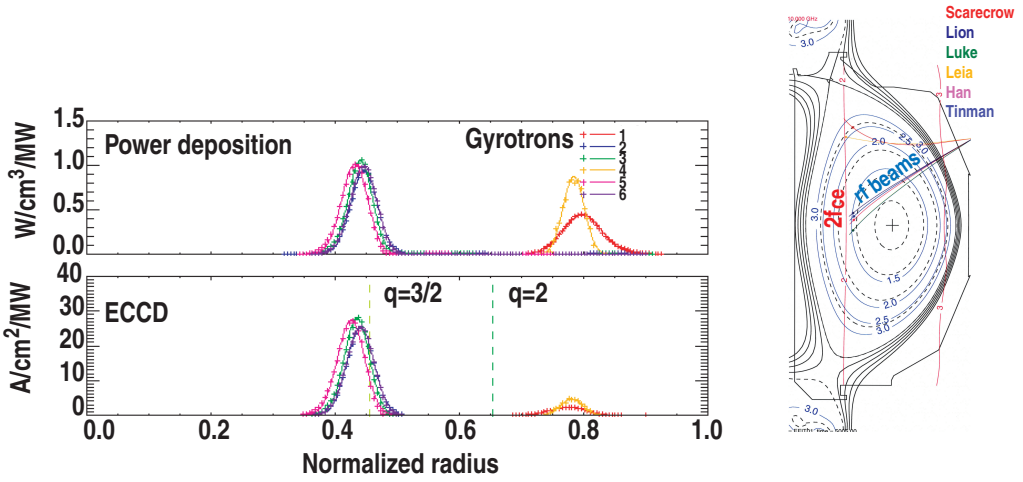

Fig. 4. The launch geometry and measured kinetic profiles are used as input to the ray tracing code, TORAY, which calculates the absorption and current drive profiles.

C. Power Supplies

The high voltage for the gyrotrons is derived from a variable ratio transformer with series/parallel strings of solid-state rectifiers. This system can deliver about 110 kVdc to tetrode modulator/regulators located in shielded and access-controlled rooms near the gyrotrons. Two of the gyrotrons have dedicated mod/regs and can be controlled independently. The remaining four gyrotrons are powered in two groups of two tubes, where two gyrotrons are powered in parallel from a single tetrode modulator. Both members of each of these pairs receive the same high voltage waveform, but there is some operational independence in that power from either can be routed into its dummy loads while its partner is injecting into the tokamak. The gyrotrons are protected against internal arcs by fast blocks which act in several μsec to remove the high voltage under fault conditions and a crowbar which fires in about $10\ \mu s$ if the high voltage block fails. The crowbar performance is checked in a wire short circuit test [24] with a 0.127 mm diameter wire to verify that at most 10 J can be delivered to the gyrotron in case of a low resistance arc. The gyrotrons can be modulated by pre-programmed waveforms with different shapes at frequencies up to about 5 kHz or can be controlled by the DIII-D plasma control system (PCS) using feedback from a number of diagnostics. For example, the electron cyclotron emission (ECE) derived electron temperature at a particular location in the plasma can be regulated by having the PCS control the modulation of gyrotrons depositing rf power on the flux surface seen by a particular ECE channel, Fig. 5.

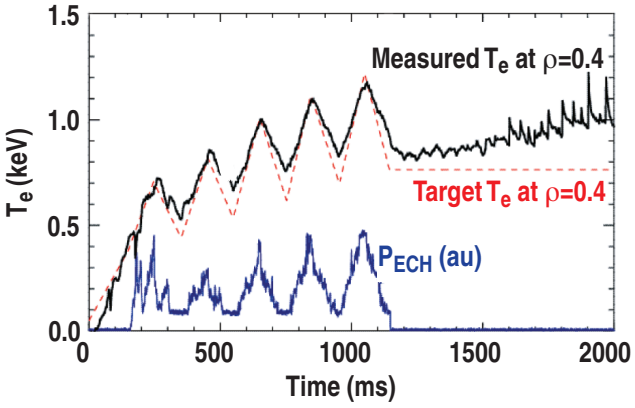

Fig. 5. The DIII-D plasma control system modulates the gyrotron output power to give a desired T_e at a particular location

The collector sweep coils are operated from 200 V audio amplifiers which have good flexibility with respect to sweep waveform and ability to handle the inductive reactance of the coils. The five gyrotron magnet power supplies, which drive the two main coils, the two orthogonal transverse coils and the gun coil, are capable of 100 A at 10 V and are designed for the superconducting magnet application with excellent stability, quench

detection and protection, and fault limit circuitry. The magnet supplies are controlled by a PC, that also provides cryomagnet temperature monitoring. The gyrotron filaments are operated from chopper regulated ac supplies having programmable ramp up and ramp down and the capability of being boosted in synchronization with the DIII-D pulse.

D. Magnets

The gyrotron magnets in the DIII-D system are of three basic types. The oldest magnet in the system requires both liquid helium (LHe) to cool the coils and liquid nitrogen (LN_2) to cool the cryostat radiation shield. This magnet has recently been retrofitted with a pulse tube reliquifier [25], which has a cold finger above the LHe reservoir that reliquifies the boiloff from the reservoir. This reliquifier has reduced the LHe consumption for that magnet to about 0.1% per day so that only one annual LHe fill is required, compared with a fill every three days previously. Full cost recovery for the reliquifier from LHe savings alone will be realized in 2-3 years. Two other magnets require regular LHe fills, but have refrigerators to cool the radiation shields, eliminating the need for LN_2. The remaining three magnets, supplied with the second group of gyrotrons, are completely cryogen-free and are cooled by compressor refrigerators delivering about 2 W of cooling power at 3.5 K to the coils. These magnets require about 60 hours for an initial cool-down to operating temperature and about 6 hours to recover from a quench occurring when the magnets are at operating field.

Because of the demonstrated risk of freezing the gyrotron in the magnet bore in case of a failure of the cryostat vacuum, the systems at DIII-D are equipped with protection against this eventuality. Wrapped around the gyrotron stalk is a flat heater plate, which is actuated by a thermal switch set to about 5ºC. The bores are also purged with a continuous low flow of dry nitrogen to provide some warming of the bore while preventing the buildup of ice that could form a bridge between the gyrotron and a cold cryostat. The compressors in the cryogen-free systems are also powered from ac supplied with a diesel backup in case of grid failure, since the time to quench is only 3 minutes if the compressors turn off when the magnets are operating.

III. WAVEGUIDE ALIGNMENT

The rf exits the gyrotron in a Gaussian beam with a waist at the CVD diamond isolation window. After exiting the gyrotron, the rf beam reflects off a single ellipsoidal focusing mirror in the MOU and enters the waveguide at a Gaussian waist, the diameter of which, 22 mm, excites the $HE_{1,1}$ waveguide mode with efficiency of about 98%. Determination of the mode content is made in several ways involving free space measurements of the rf beams following passage through a length of waveguide and direct measurement using a mode analyzer miter bend. The single mirror has a three-point tilt system with precision micrometers that can tilt the mirror in two directions and translate it parallel to the rf beam axis. Although alignment is simpler with a single mirror than with a two-mirror MOU, this scheme does not allow parallel motion of the rf beam relative to the waveguide in the vertical plane. Simply adjusting the tilt of the mirror with micrometers can accurately place the beam at the center of the waveguide but with unknown tilt relative to the waveguide axis.

At DIII-D, a setup procedure is used for each gyrotron when it first is operated. The rf beam is propagated into free space for short pulses a few ms in length and hits a paper target placed at a series of locations about 10 cm apart along the beam as it travels away from the gyrotron [26]. Infrared images of the target are made, the sequence of which is subjected to phase retrieval analysis [27,28], which yields both the propagation angle with respect to the gyrotron output flange and the transverse offset of the beam center at the gyrotron output window. This defines the optical axis of the rf beam coming from the gyrotron and also serves as a check on the beam quality, which provides the data to design the MOU mirror. Once the tilt and offset of the beam are known, a specialized spool piece with correct offset and tilt is made to connect the gyrotron to the MOU. The spool piece places the axis of the rf beam onto the optical axis of the MOU and rf beamline. Without this procedure, the single mirror MOU cannot be guaranteed to work.

For some of the lines in the DIII-D installation, mode conversion of 5%–10% in the first several meters of the waveguide indicated that the procedure described here did not simultaneously produce the accuracy of ±0.6° in tilt and ±1.2 mm in centering necessary to achieve <1% mode conversion [29].

Because reflections from the waveguides and flanges can interfere with the measurement of the beam profile during alignment and there was excessive mode conversion at the input end of the waveguide, an improved procedure is now used, which adds an additional step following the manufacture of the specialized spool piece and MOU mirror. A second free space propagation is now performed for the rf beam after reflection from the mirror. With the waveguide removed, the mirror is adjusted to align the rf beam parallel to the waveguide axis and as close to the location of the center of the waveguide as possible. The waveguide is then put in place and small adjustments to the MOU mirror position and tilt are performed. Power profile measurements are

then made at several distances from the input using an infrared camera or thermally sensitive paper for a beam propagating into free space after a section of waveguide about 1 m to 2 m in length. A phase recovery analysis of the beam propagating into free space after transiting the waveguide gives the mode content of the rf beam which resulted from the coupling at the waveguide input. Using this procedure results in an $HE_{1,1}$ content of the beam in the waveguide as high as 92%, which represents excellent coupling and results in an rf beam that has the theoretical transmission efficiency of 80%, (-1 dB) for the entire waveguide run. The measured mode contents for the waveguides in the DIII-D system are summarized in Table 2. It was found that an optical alignment using a laser and thin front surface mirrors attached to the MOU mirrors was not as successful as performing the hot test alignment described here.

Table 2. After the transverse and tilt alignment of the rf beams at the waveguide input have been completed, the excited modes are calculated from infrared power profile measurements as the beams propagate into free space after passage through a short length of waveguide and a phase retrieval analysis of the profiles. The LP modes form a convenient basis set for describing the linearly polarized beam. The LP_{01} mode corresponds by definition to the $HE_{1,1}$ mode. Other order LP modes represent combinations of HE, EH and TM modes with higher orders, which indicate mode conversion due to misalignment, imperfect mode purity in the generated beam from the gyrotron or the 98% theoretical coupling efficiency between a perfect Gaussian beam and $HE_{1,1}$. The cases with $HE_{1,1}$ percentage near 90% represent very good alignment with low mode conversion.

Gyrotron	$HE_{1,1}$ (%)	$LP_{1,1}$ (e) (%)	$LP_{1,1}$ (o) (%)	$LP_{1,2}$ (o) (%)	$LP_{1,2}$ (o) (%)	$LP_{0,2}$ (%)	$HE_{1,3}$ (%)	$LP_{1,3}$ (e) (%)	Others (%)
Tinman	87.3		1.0			5.7			6.0
Scarecrow	88.3	2.2	1.9	0.8					6.8
Lion	92.0	2.3	0.5	1.0	0.6	0.6	0.2		2.8
Luke	84.6	1.2	2.5	0.3	0.1	4.9	0.9	0.3	5.2
Han	90.9	0.4	0.5	0.2	0.2	3.2	0.4		4.2
Leia	87.0	5.2	3.2			0.4			4.3

The measured $HE_{1,1}$ fraction does not correlate perfectly with the overall efficiency of a transmission line as can be seen in Table 3, where performance parameters are presented along with the measured $HE_{1,1}$ content from Table 2. Nevertheless, the line with the poorest mode purity, on the Luke system, also has the largest MOU loss and nearly the largest waveguide heating near the input. Uncertainties in the phase retrieval process, the infrared beam profile measurements, the calorimetry measurements and the localized nature of waveguide heating can all contribute to the discrepancy.

Although the theoretical coupling from a perfect Gaussian beam to waveguide carrying the $HE_{1,1}$ mode is 98%, the beams produced by the gyrotrons have more like 95% Gaussian content, leading to a maximum $HE_{1,1}$ purity in the waveguide of about 93%. No phase correction is presently done with the MOU mirrors although this is also possible. Recent improvements in the designs of mode converter/launchers in gyrotrons [30,31] have increased the possible

maximum Gaussian mode purity to over 99% so that the next generation of gyrotrons in the DIII-D system will couple a larger fraction of the generated power.

Table 3. The waveguide line losses measured in high power tests do not correlate perfectly with the measured fraction of $HE_{1,1}$ but the worst system for waveguide transmission does also have the lowest $HE_{1,1}$ mode content. Based on these measurements, a new MOU coupling mirror is being manufactured for the Luke system. The theoretical loss is based on the length of the line and the number of miter bends. The waveguide temperature is the maximum change for measurements made at several points in the first few meters of each line and does not represent an average. Maximizing the waveguide transmission efficiency is a continuing project.

Gyrotron	HE_{11} Mode Content (%)	Measured Loss in Waveguide Line (dB)	Theoretical Loss in Line (dB)	Max ΔT Waveguide for 1 s Pulse (°C)	Loss in MOU (%)
Tin Man s/n 102	87	0.91	0.98	2.0	2.8
Scarecrow s/n 101R	88	1.46	0.98	5.0	3.8
Lion s/n 103	92	1.04	0.98	2.3	3.3
Luke s/n 104	85	1.51	0.98	4.0	7.9
Han s/n 105	91	1.11	0.98	2.5	4.5
Leia s/n 106	89	1.03	0.89	2.5	5.4

The transmission line efficiencies are measured directly by moving a large dummy load between the ECH gyrotron vault and the DIII-D machine pit and referencing the calorimetrically measured power in the dummy load to calorimetry on the gyrotron cooling circuits, the internal loads and cavity, which are proportional to the generated power. Once the correlations among gyrotron calorimetry, rf beam quality and transmitted power are established, a calibrated value for injected rf power at the tokamak can be quoted for every plasma shot. A monitor of this power has also been developed to provide a real time measurement of the quality of the rf beam in the waveguide at the tokamak.

The beam monitor miter is a four port miter bend beam splitter with -57 dB pickoff fraction, that can be used to determine both the power in the $HE_{1,1}$ main mode by measuring and summing both orthogonal polarizations and to measure primary contaminant modes, $HE_{2,1}$ and $TE_{0,1}$, that are generated by misalignments. This miter is shown in Fig. 6, along with traces showing the time dependence of the measurements for the different signals. The monitor measures the $HE_{1,1}$ mode and contaminating $HE_{2,1}$ and $TE_{0,1}$ modes as seen in the upper set of traces. In the lower set of traces the two orthogonal linearly polarized components of the $HE_{1,1}$ mode are presented along with a very low amplitude $HE_{2,1}$ signal. Near the tokamak, after about 80 m of waveguide, it is expected that most of the higher order modes will have damped out, leaving primarily the $HE_{1,1}$ mode. Infrared measurements of the rf beam launched into the tokamak and comparison of

the signals for the long waveguide and for measurements near the MOU verified that this is indeed the case. Measurements of the $HE_{2,1}$ and $TE_{0,1}$ fractions during intentional misalignment of the MOU mirrors showed that the miter monitor provides an accurate measure of the beam quality. So, improving the alignment or checking for problems with the transmission lines becomes a matter of observing the miter signals in real time once the full power long pulse dummy load measurements near the tokamak have calibrated the device.

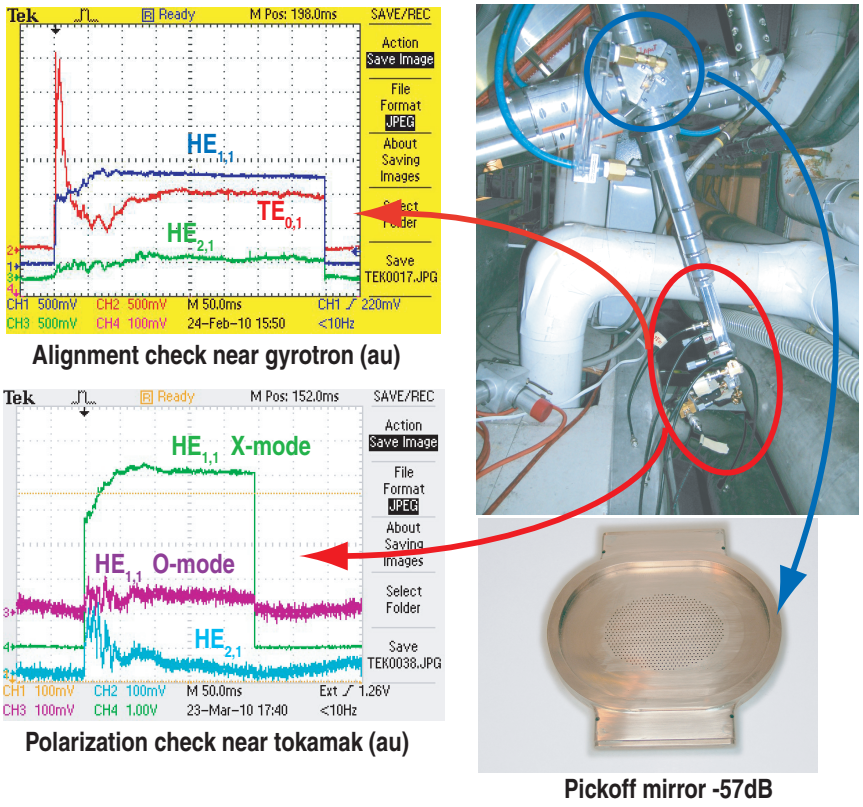

Fig. 6. A four port power/mode monitor with -57 dB pickoff mirror is used to diagnose the mode content of the rf power in the waveguide and the power in the two orthogonal polarizations to provide a calibrated power measurement at the tokamak and a check of the polarizer performance. Examples of the mode contamination and linear polarization measurements are shown in the upper and lower parts of the figure.

IV. LAUNCHERS

The DIII-D installation presently has three launchers, Fig. 7, each of which handles the power from two gyrotrons with independent steering. Approaching the launchers, the 31.75 mm diameter waveguides uptaper to 63.5 mm diameter and in the DIII-D vacuum vessel the rf beams pass into free space where they are weakly focused by a 45° mirror onto a fully articulating flat mirror, that directs the rf beams over a 40° scan range poloidally and ±20° toroidally providing both co- and counter-current drive anywhere in the tokamak upper half plane. The steering mirrors both rotate and tilt, so scan motions in the two directions are not orthogonal. The angles for both motions are read by 14 bit encoders so that positions of the mirrors can either be determined in real time during a plasma discharge or calculated by an offline computer code for any allowable combination of steering inputs. Based on the equilibrium and aiming, the power deposition and current drive are calculated. At present, the more critical poloidal motion is accomplished using dc electric motors, which can cover the full 40° poloidal scan range in about 3.5 s, 11.4°/s, or about 40 cm/s for a typical DIII-D equilibrium, with a positional accuracy of ±0.1° or about 3.5 mm vertically. In the toroidal direction, the motors are air turbines with about the same slew rates but approximately a factor of 20 worse positional accuracy. The toroidal drive turbine motors are being replaced by electric motors but in the interim the drives can be set manually for the rare experiments where high accuracy is required toroidally. For comparison, the rf beam footprint is about 10 cm in diameter at the -10 dB contour at the center of the tokamak. No problems have been encountered as a result of having the electric motors located within 1 m of the DIII-D toroidal field coil including during real time tests when the motors were operated while the toroidal field coil was energized. Suppression of the $m/n = 3/2$ neoclassical tearing mode (NTM) as the rf power was swept across the $q = 1.5$ resonant surface under PCS control is shown in Fig. 8.

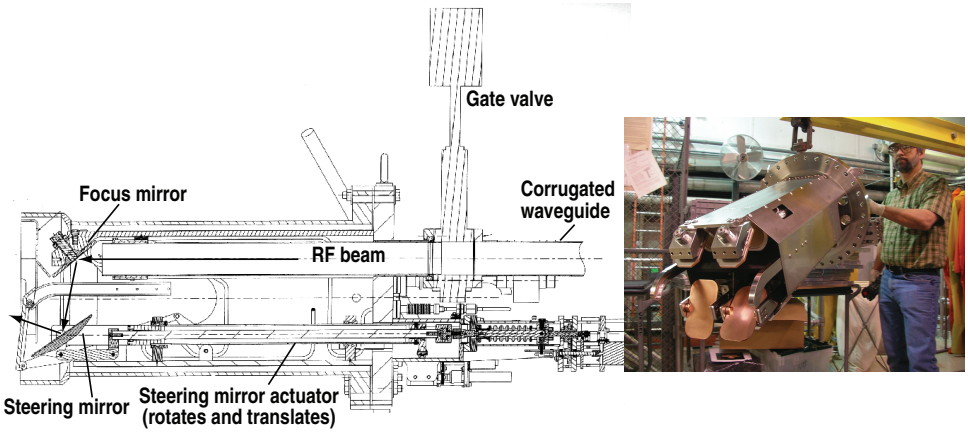

Fig. 7. The launchers in the DIII-D system both focus and steer the rf beams.

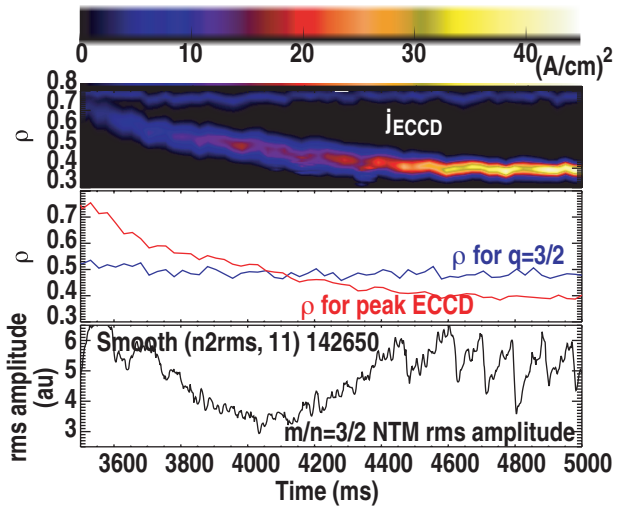

Fig. 8. Suppression of the $m/n = 3/2$ NTM by sweeping the ECCD region across the $q = 1.5$ under PCS control demonstrates the real time control of the injection geometry.

The mirrors are not actively cooled, relying on radiation and conduction for cooling between gyrotron pulses. Measurements of the mirror temperatures using resistance temperature devices (RTDs) during plasma pulses allow the surface temperatures to be inferred [32]. From Fig. 9, it can be seen that heat loading of the mirrors from plasma radiation is approximately as important as direct heating by the rf beams and that the temperatures of the front surfaces of the mirrors are calculated to be about 500ºC, provided sufficient cool down time is allowed. After extensive operation, however, several mirrors were found to have indications of higher heating and in two cases focusing mirrors suffered major damage. In one such case, minor melt damage was seen during a short machine vent, but time did not permit replacement of the mirror. After 269 additional shots with a variety of pulse lengths several seconds long, the surface was completely melted through the copper and stainless steel down to the mounting stud. Additional thermal modeling showed that the poor heat transfer due to the stainless steel mounting stud plus a hole drilled in the back of the mirror for an RTD combined to cause the thermal runaway. Signs of heating were also observed in the flat steering mirrors, which have a laminated stainless steel and copper construction that provides better heat transfer away from the copper reflecting surface than for the focus mirror design. The focus mirrors and steering mirrors are being upgraded to a design with improved thermal transfer capability, but still will not be actively cooled.

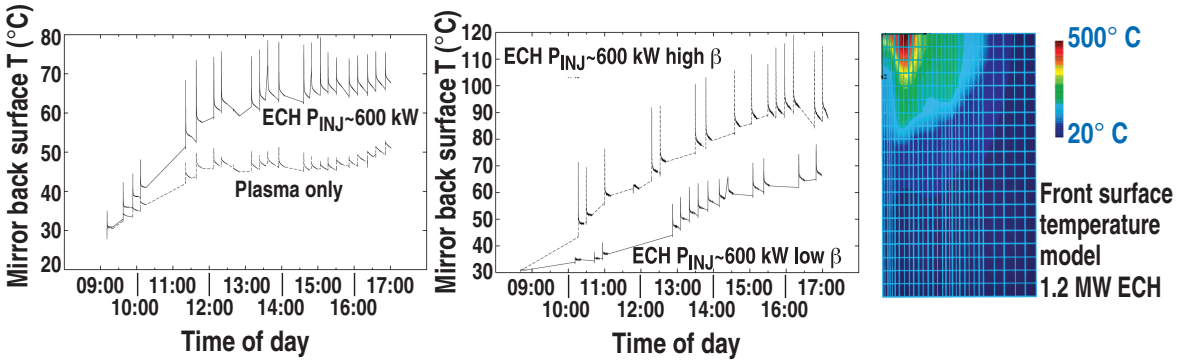

Fig. 9. Thermal performance of the launcher mirrors. The model calculations indicate a worst-case surface temperature of 500ºC for a 5 s gyrotron pulse at 1.2 MW. Mirror heating by radiation from the plasma is approximately as important as heating by the rf beam.

There has been one catastrophic launcher failure on the DIII-D system in which an rf driven arc was repeatedly struck at the mouth of the launcher waveguides. The arc was undetected until problems with the tokamak discharge led to a spectroscopic survey that found aluminum in the plasma. Upon opening the tokamak and inspecting the launchers, it was discovered that, through an assembly error, the actuator rod on a carbon composite shutter on one launcher was slowly changing its length and eventually the shutter was not fully retracting. The rf beam was striking the edge of the shutter, vaporizing carbon and then driving an arc for the duration of the rf pulse. Approximately 10 cm of the ends of both waveguides on the launcher were melted completely and an additional 10 cm long slot in the horizontal plane on the waveguides was also melted. As a result of this, video cameras were mounted on the launchers, Langmuir probes were installed to detect plasma at the launcher waveguides and the shutters were removed. The aluminum launcher waveguides also were replaced with stainless steel guides silver plated on their inside diameters. The Langmuir probe interlocks occasionally trip during extremely high-density tokamak operations such as when pellets or massive gas bursts are being injected or when a disruptive termination occurs. Aside from isolated discoloration in the new waveguides, no further damage has been noted and there has been no deterioration of the mirror surfaces resulting from removal of the shutters.

V. CONTROL SYSTEM

The DIII-D ECH gyrotrons operate under a flexible control system in which functions are distributed among a number of computers and monitors [33]. The slowest of these is a programmable logic controller (PLC) system, which handles the status and commands for gate valves, waveguide switches, vacuum, cooling, gyrotron magnets, high voltage commands and other low speed interlocks and commands which can tolerate the approximately 20 ms PLC cycle times. Some of the PLC functions, such as opening and closing waveguide gate valves, normally reside in the DIII-D vacuum control system computer, but these can be overridden by the ECH PLC system so that, for example, the gate valves cannot be opened by the DIII-D system if the waveguide pressure exceeds 1.3×10^{-3} Pa.

Each gyrotron has its own computer, a PC running Windows XP in PXI configuration. Each magnet is controlled by a local PC running Windows XP and data acquisition is performed by a data server also running Windows XP. The PLC interface computer runs under Windows 98. A control server orchestrates the operation of the entire system and interfaces to the operators through a LabVIEW user interface. Gyrotrons can be operated in "group" mode in which commands apply to any desired subset of the full complement of tubes. This allows timing commands to be sent to all gyrotron control computers simultaneously or to separate the system as desired. The group mode is prohibited for setting filament parameters, since individual gyrotrons have different filament voltage commands for normal operation at 40 A, 80 kV. Filament boost, as discussed above, is a part of the filament command syntax and allows the filament voltage to be increased by about 10% at a variable time, averaging 8 s, before the gyrotron pulse. For gyrotrons running quasi-continuously, the filament boost can be applied as required during the pulse, but for the intermediate length pulses used in the DIII-D system, this boost must be pre-programmed so that cathode cooling and the boosted heating offset each other.

The pulse timing is handled by a programmable waveform generator on each system, which can be set up in several modes. A continuous output followed by modulated pulses, modulated pulses followed by continuous output and continuous modulation, square wave, sine wave or triangular, for an arbitrary number of pulses and for pulse lengths up to 5 s are available. Modulation under the control of the PCS can be selected. For this mode, the PCS sends an analog voltage on optical fibers from the DIII-D control room to the ECH control system for each gyrotron. The full range of gyrotron output power is obtained for a high voltage range of about 60–80 kV. Therefore, the baseline for PCS modulation must be shifted so that 0 V corresponds to ~60 kV in the gyrotron control system and 10 V provides full output voltage. The modulation limits are gyrotron dependent and these ranges differ for the various gyrotrons. Under either form of control, the desired waveforms provide the control inputs to the HV power supplies. Triggering is initiated by receipt of a hexadecimal code from the DIII-D master clock system, which triggers a timing generator that is set by the gyrotron control system.

Fault processing is handled either by a discriminator/trigger module or, for the two newest systems, by a field programmable gate array (FPGA) system. Based on a year of reliability testing and extensive operational experience with the new FPGA installations, all control and fault processing is presently being migrated to FPGA format. The FPGA greatly increases the flexibility of the system, permitting arbitrary programming of output power waveform, retry after fault, response to incipient fault and variable fault response, all of which increase the operational reliability and flexibility of the system and which, in particular, improve the ability to condition gyrotrons as they are placed in service.

The data acquisition system has redundant digitizers for waveforms and archives calorimetry data from a number of circuits on the gyrotrons and transmission lines which enable generated rf power to be determined and sent to the DIII-D database for every shot.

Following this overview of the components of the ECH system, we now turn to providing performance data, test results and more details of some of the subsystems.

VI. GYROTRON RELIABILITY

Gyrotrons are being incorporated into all the next generation tokamak devices due to their demonstrated ability to provide accurate localization of heating and current drive, their small launcher footprint per unit power, their electrical efficiency, their immunity to coupling problems resulting from plasma shape and ion species and the fact that the gyrotrons can be located some distance from the tokamak outside the radiation shield without appreciable performance penalty. Continuous operation at generated power levels of 1 MW, several second operation at 1.5 MW and short pulse operation at over 2 MW have all been demonstrated for frequencies above 100 GHz, which are relevant to magnetic fusion devices.

With available unit power certain to increase, and with cw performance certain to become routine, the suitability of gyrotrons for heating and current drive in power producing reactors is clear. The question becomes one of reliability at maximum operating parameters. The six-gyrotron DIII-D installation is being used daily for experiments which call for pulse lengths up to 5 s and maximum possible generated power. The installation has been in a continual state of development until the most recent campaign, when power supplies had become relatively reliable and all the gyrotrons had been conditioned for reliable performance at 5 s pulses, 80 kV and 40 A.

Reliability is calculated for the DIII-D system on a gyrotron by gyrotron basis, so if an experimenter requests six gyrotrons and one faults, the system reliability for that shot would be calculated as 83%. Because some experiments require power scans and some tokamak shots have problems although the gyrotrons ran perfectly, this accounting algorithm represents a reasonable compromise reflecting the real utility of the system. The reliability of the DIII-D system has hovered at about 85% for the past 5 years, Fig. 10, despite commissioning of new power supplies, conditioning of new gyrotrons and returning repaired gyrotrons to service, which can require conditioning, often during experimental operations. Similar reliability was obtained in a landmark performance study using the ITER scenario of 600 s pulses repeated every 30 min at JAEA [34]. For the DIII-D system, the most problematic operations involve modulation by the plasma control system and pulses between 3 and 5 s in length. With PCS control, particularly with feedback, rather than pre-programmed operation, the tubes can be commanded to operate for relatively long periods in regimes with low rf output but large electron beam currents at high voltage. These regimes can load the collector excessively. It should be noted that gyrotron operations are coupled by common power supplies and by common daily startup issues, therefore it is not correct to infer from the reliability studies that ITER gyrotron system reliability will be 0.85^{24}.

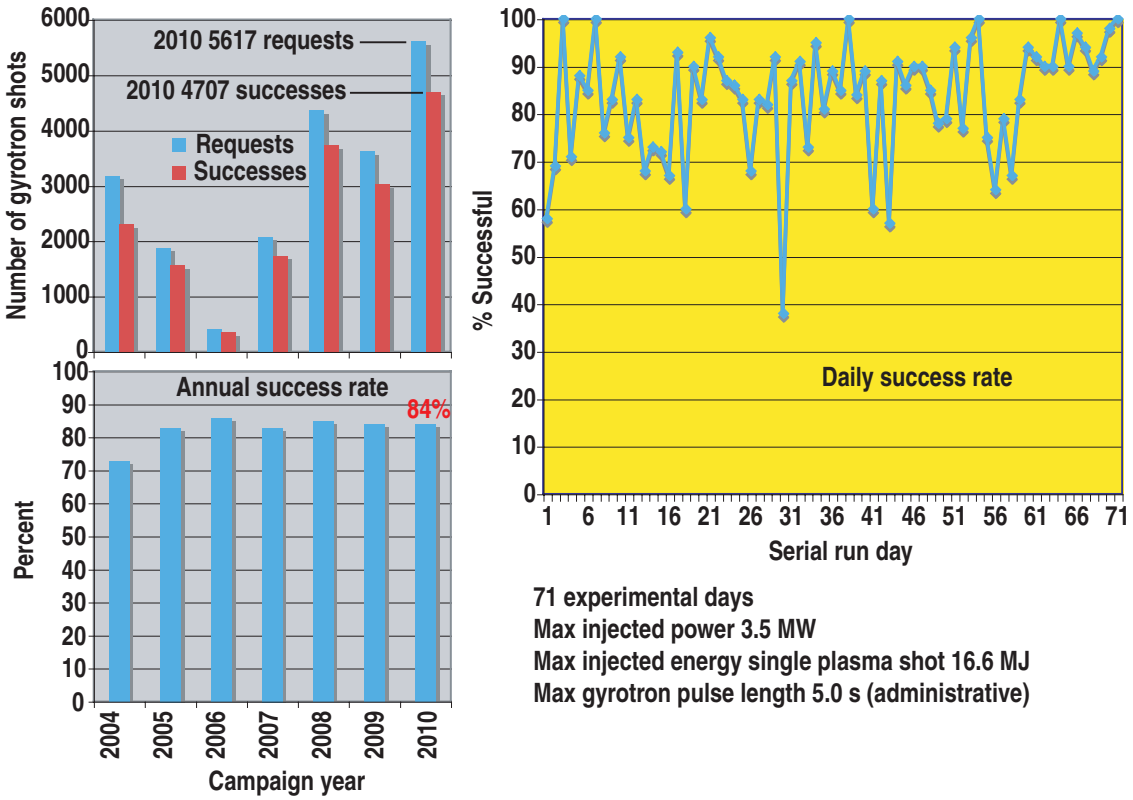

Fig. 10. Reliability of the individual gyrotrons in the DIII-D installation has been about 85% as the system was being installed and upgraded. The faults are not randomly distributed. Most faults occur during the daily startup when the system parameters are being tuned. Because four of the gyrotrons are run in pairs from single high voltage power supplies, a single fault will cause two gyrotrons to block.

With intermediate pulse lengths between about 3 and 10 s in length, cathode cooling from electron emission during the pulse requires boosting the filament voltage by at least 10% several seconds before the pulse to maintain the electron beam current. Operating at maximum rf output power with boosted filament requires continuing adjustment and occasionally results in loss of rf generation and a fault, which decreases the overall reliability during tune up. For shorter pulses, cathode cooling is not a factor and for longer pulses the filament can be adjusted precisely during the pulse. Interestingly, most faults in the DIII-D system derive not from gyrotron problems once the tubes are well conditioned, but from problems with the high voltage power supplies involving instability, high voltage measurement, gyrotron filament control and changes in the unregulated supply voltage due to loading of the power grid during tokamak pulses. This latter effect has implications for the design of the high voltage power supplies to maximize the width of the operating window and minimize the sensitivity of the supplies to variations in the dc supply voltages. System operating parameters determined when the tokamak is not operating can be different from those required during a plasma pulse. In order to operate the DIII-D gyrotrons with acceptable reliability, the generated rf power during experiments is typically derated by about 15% from the maximum.

The gyrotrons present nonlinear loads to the power supplies. It was found that a single modulator could drive a purely resistive load at 80 kV and 80 A, but when two gyrotrons, each drawing 40 A at 80 kV, were operated in parallel from the same modulator, the regulation was unstable. Power supply regulation problems can cause faults either because the output voltage fails to track the command or because the rapidly changing displacement currents in the supply cable can be erroneously interpreted by the fault system as body current or arc faults. Independent of the fault circuitry, the gyrotrons themselves, especially when operated at close to maximum power, do not tolerate fluctuations, and particularly not increases, in the operating voltage. The solution to this was to operate the modulator tetrode supplying two gyrotrons at a filament voltage near or slightly below the low end of its specification range. The tetrodes require an input voltage at least 6–8 kV above the requested gyrotron voltage for proper regulation. At the beginning of a pulse, when the cables are being charged, the short-term current drain can exceed the capability of the supply. To help support the input voltage transiently, a 20 μF capacitor bank is connected in parallel with the dc supply voltage. One limit on the capacitance of this bank is determined by the requirement for <10 J fault current in case of a gyrotron arc. A higher supply voltage, which could be used instead of the capacitor bank to counteract the voltage sag under load, puts more strain on the tetrode in its regulation function and can result in uncommanded crowbars and breakdown in the power supply enclosures. So the systems run in a voltage window which occasionally can be narrow and can result in unreliable gyrotron operation for experiments.

Improvements to the power supply system to address these issues are being installed. The size of the capacitor banks is being doubled in a design that has passed the 10 J test, the crowbar standoff voltages are being increased by use of an experimental solid-state switching unit and the gyrotron filament power supplies are being replaced by programmable supplies with regulated sinusoidal, rather than chopped, outputs.

VII. GYROTRON DIAGNOSTICS

In addition to the four-port miter, several diagnostics have been developed for the DIII-D system to help diagnose gyrotron performance. These include a spectroscopic diagnostic of the light emanating from a tube during conditioning and a new method of measuring the injected power in the tokamak.

A. Spectroscopy

Spectroscopy can provide information about the source of gas in the gyrotron during conditioning. A visible spectrometer was positioned to observe the light passing through the CVD diamond window on a gyrotron being conditioned. A response test using a fluorescent lamp showed good sensitivity for wavelengths greater than about 520 nm. A pair of typical spectra are compared in Fig. 11, one for a normal conditioning pulse which ran through to the requested 500 ms pulse length and a second which tripped the system overcurrent interlock due to an internal arc. The spectrum during a normal pulse has a broad continuum with very little structure. But, during the arc shot, line structure is visible. As expected for a device which was brazed in a hydrogen furnace, a strong hydrogen line at 656.2 nm is seen, but there also is clear evidence of Ti from the Ti^{I} doublet at 588 nm and the Ti^{I} line at 674.3 nm, possibly broadened by C^{I}. The only sources of Ti in the CPI gyrotrons are the vacion pumps, so the spectra suggest that arcing and possible reflux of gas from these pumps contribute to the deconditioning observed during such an arc shot.

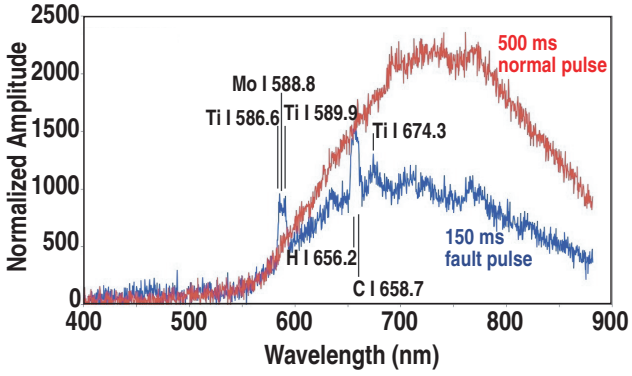

Fig. 11. The visible spectra of light emanating from a gyrotron during normal operation and during a fault show Ti and H lines increase during the fault pulse.

B. Injected Power

Injected power at the tokamak is a surprisingly difficult measurement to make for full performance operation. A power calibration can be made by switching to a short pulse dummy

load at the tokamak, by measuring the transmission line efficiencies and relating the generated power determined from gyrotron calorimetry to the power eventually arriving at the tokamak or by constructing some type of heavily attenuating rf pickoff device which is able to handle high power, long pulses and various propagating modes installed near the tokamak. It was discovered by chance that on DIII-D the calibrated bolometer arrays, which are usually used to provide measurements of total radiated power and spatially resolved measurements from tomographic analysis can also provide the injected power measurement for the ECH system under certain circumstances. In Fig. 12, a test shot is presented in which ECH power from different combinations of gyrotrons was measured by the bolometers with good agreement between the bolometric measurement and the calibrated injected power determined from measured transmission line efficiency combined with gyrotron performance data. The linearity check also shown in the figure gives the surprising result that the measurement is valid with or without a resonance in the vessel as long as there is sufficient gas for breakdown. There also are some requirements on gyrotron aiming for best agreement, which are believed to be important because of the tomographic algorithm, optimized for diverter measurements, which is used in the analysis of the bolometric data.

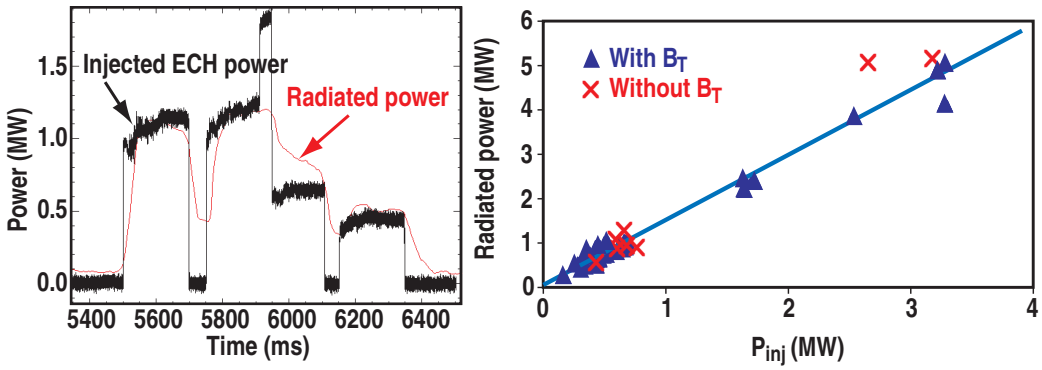

Fig. 12. A bolometric measurement of the power in the vacuum vessel without plasma can give a good indication of the injected rf power.

VIII. FUTURE PLANS

The long-term plan for the ECH system on DIII-D calls for an increase in both injected power and pulse length. This plan will be executed in stages, the first step being the improvement in the performance of the present system. Because miter bends account for a large fraction of the transmission losses, the transmission lines are being rerouted by removing the crossover gallery, which previously permitted the connection of any gyrotron to any launcher. This will reduce the number of miters from 72 to 58, giving approximately 200 kW additional injected power at nearly no cost. The mode conversion loss at each gyrotron can also be reduced substantially [35,36]. A miter bend is being designed for the DIII-D transmission line that is nearly a direct replacement for the present miters, but that reduces the mode conversion from about 1.5% to less than 0.3% with good bandwidth performance over the range of frequencies presently in use and planned for the DIII-D system. We also are improving the alignment of the rf beams into the waveguides as discussed above and plan to replace all the miter bends in the system with lower loss designs. Longer term, we are increasing the number of gyrotrons in the complex and are increasing the generated power per gyrotron. The first stage in this process has been funded and will add a 7th 110GHz depressed collector gyrotron to the system, with output power of 1.2–1.3 MW. This project will include construction of the required high voltage power supply to handle two gyrotrons, an additional dual launcher, plus the transmission line and control system for one gyrotron. The project will increase the size of the gyrotron vault at DIII-D to accommodate the installation.

In parallel with preparations for this gyrotron, a program to develop a higher power tube designed for 1.8 MW and reliably generating 1.5 MW at approximately 117 GHz is being initiated. This tube will use some of the infrastructure installed at the time of the upgrade to seven gyrotrons, with the addition of a new transmission line and controls. The gyrotron will be the first of a group that will be intended to replace the current gyrotrons as they approach the ends of their service lives. Physics requirements [37] call for approximately 12 MW injected rf power, therefore the long term plan includes a 5th dual launcher and eventual increase in the number of gyrotrons to 10, all of which will be capable of generating in excess of 1.5 MW, yielding an injected rf power ≥12 MW, when transmission line losses are taken into account.

REFERENCES

[1] R. Prater and A.J. Lieber, "Heating effectiveness in the electron cyclotron heating experiments in the Doublet III tokamak," Proc. 5th Int. Workshop on Electron Cyclotron Emission and Electron Cyclotron Heating, Eds. Ronald Prater and John Lohr, General Atomics Report GA-A18294 (1985).

[2] R.A. James, *et al.,* Phys. Rev. A **45**, 8783 (1992).

[3] M. Bornatici, *et al.,* Nucl. Fusion **23**, 1153 (1983).

[4] R. Prater, *et al.,* Plasma Phys. Control. Fusion **35** (1993).

[5] John Lohr, *et al.*, Phys. Rev. Lett. **60**, 2630 (1988).

[6] John Lohr, *et al.*, "Recent electron cyclotron heating experiments with low field launch of the ordinary mode on the DIII-D tokamak," Proc. 7th Joint Workshop on Electron Cyclotron Emission and Electron Cyclotron Resonance Heating, Hefei, China (IAEA, Vienna 1990) p. 157.

[7] R.W. Callis, *et al,* "Initial results from the multi-megawatt 110 GHz ECH system for the DIII-D tokamak," Proc. 12th Topical Conf. on Radio Frequency Power in Plasmas (1997) p. 191.

[8] G.G. Denisov, *et al.,* Int. J. Electronics **72**, 1079 (1992).

[9] Kevin Felch, *et al.*, IEEE Trans. Plasma Sci. **24**, 558 (1996).

[10] Y. Gorelov, *et al.,* "Infrared monitoring of 110 GHz gyrotron windows at DIII-D," Proc. 12th Joint Workshop on Electron Cyclotron Emission and Electron Cyclotron Heating, Ed. Gerardo Giruzzi, World Scientific, Singapore (2002) p. 461.

[11] J. Lohr, *et al.,* "The 110 GHz gyrotron system on DIII-D: Gyrotron tests and Physics results," Proc. Strong Microwaves in Plasmas (2000) p. 46.

[12] G.G. Denisov, *et al.*, "Phase corrector synthesis and field measurements for gyrotron quasi-optical beams," Proc. 20th Int. Conf. on Infrared and Millimeter Waves (1995) p. 483.

[13] J.R. Brandon, *et al.,* Fusion Eng. Design **53**, 553 (2001).

[14] C.B. Baxi, *et al.,* Fusion Eng. Design **82**, 731 (2007).

[15] M. Joung, "Commissioning and operation of 110 GHz ECH system in KSTAR," accepted for publication in Proc. 16th Joint Workshop on Electron Cyclotron Emission and Electron Cyclotron Heating, Ed. Jiangang Li, World Scientific, Singapore (2010).

[16] Hiroaki Shoyama, *et al.,* Jpn J. Appl. Phys. **40**, 906 (2001).

[17] Kevin Felch, *et al.,* Nucl. Fusion **48**, 1 (2008).

[18] John Lohr, *et al.,* Fusion Sci. Technol. **48**, 1226 (2005).

[19] F. Leuterer, *et al.,* "Planning, construction and operation experience of the ASDEX-Upgrade ECRH system," Proc. 15th Joint Workshop on Electron Cyclotron Emission and Electron Cyclotron Heating, ed. John Lohr, World Scientific, Singapore (2009).

[20] J.L. Doane, "Propagation and mode coupling in corrugated and smooth-wall circular waveguides," Ed. K.J. Button, Academic Press, Infrared and Millimeter Waves **13**, 123-170 (1985).

[21] J.L. Doane, "Compact $HE_{1,1}$ to surface wave convertors for high power waveguide dummy loads," Int. J. Infrared Millimeter Waves **14**, 363 (1993).

[22] L.L. Lao, *et.al.*, "MHD equilibrium reconstruction in the DIII-D tokamak," Fusion Sci. Technol. **48**, 968 (2005).

[23] K. Matsuda, "Ray tracing study of the electron cyclotron current drive in DIII-D using 60 GHz,": IEEE Trans. Plasma Sci. **17**, 6 (1989).

[24] S.G.E. Pronko and T.E. Harris, "A new crowbar system for the protection of high power gridded tubes and microwave devices," General Atomics Report GA-A23652, http://web.gat.com/pubs-ext/MISCONF00/A23652.pdf

[25] Gifford-McMahon pulse tube cryocooler from Cryomech, 113 Falso Dr., Syracuse NY, USA.

[26] Takahashi Shimozuma, *et al.,* J. Plasma Fusion Res. **81**, 191 (2005).

[27] A.V. Chirkov, *et al.,* Opt. Comm. **115**, 449 (1995).

[28] J.P. Anderson, *et al.*, "Phase retrieval of gyrotron beams based on irradiance measurements," IEEE Trans. Microwave Theory Techniques **50**, 1526 (2002).

[29] K. Ohkubo, *et al.,* J. Infrared Millimeter and Terrahertz Waves **18**, 23 (2007).

[30] Jeffrey Neilson, "Optimization of Quasi-Optical Launchers for Multi-Frequency Gyrotrons," IEEE Trans. Plasma Sci. **35**, 6 (2007).

[31] Michael P. Perkins, *et al.*," A High Efficiency Launcher and Mirror System for Use in a 110 GHZ $TE_{22,6}$ Mode Gyrotron," Int. J. Infrared and Millimeter Waves **28**, 207 (2007).

[32] K. Kajiwara, *et al.,* Proc. of 20th IEEE/NPSS Symposium on Fusion Engineering, San Diego, California, Institute of Electrical and Electronics Engineers, Inc., Piscataway, New Jersey (2003).

[33] D. Ponce, *et al.,* "The DIII-D Multiple Gyrotron Control System," Proc. of 19th IEEE/NPSS Symposium on Fusion Engineering, Atlantic City, New Jersey, Institute of Electrical and Electronics Engineers, Inc., Piscataway, New Jersey (2002) p. 184.

[34] K. Sakamoto, *et al.*, "Development of high power long pulse ITER gyrotrons," Proc. 16th Joint Workshop on Electron Cyclotron Emission and Electron Cyclotron Heating, Ed. Jiangang Li, World Scientific, Singapore (2010).

[35] J.L. Doane and C.P. Moeller, "$HE_{1,1}$ bends and gaps in a circular corrugated waveguide," Int. J. Electronics **77**, 489 (1994).

[36] V.I. Belousov, *et al*., "Improved multi-function miter bends for corrugated waveguides of high power millimeter-wave transmission lines," Proc. Int. Workshop Strong Microwaves in Plasmas," Ed. A.G. Litvak, Russian Academy of Sciences, Nizhny Novgorod **1**, 264 (2003).

[37] Timothy C. Luce, IEEE Trans. on Plasma Sci. **30**, 734 (2002).

ACKNOWLEDGMENT

This work was supported by the U.S. Department of Energy under Cooperative Agreement DE-FC02-04ER54698.